1994-06

Wave reflections from breakwaters

Dickson, William S.

Monterey, California. Naval Postgraduate School

NAVAL POSTGRADUATE SCHOOL
Monterey, California

THESIS

WAVE REFLECTIONS FROM BREAKWATERS

by

William S. Dickson

June, 1994

Thesis Advisor: T. H. C. Herbers
Co-Advisor: E. B. Thornton

REPORT DOCUMENTATION PAGE

Form Approved OMB No. 0704-0188

1. AGENCY USE ONLY *(Leave blank)*	2. REPORT DATE June, 1994.	3. REPORT TYPE AND DATES COVERED Master's Thesis

4. TITLE AND SUBTITLE WAVE REFLECTIONS FROM BREAKWATERS

5. FUNDING NUMBERS

6. AUTHOR(S) William S. Dickson

7. PERFORMING ORGANIZATION NAME(S) AND ADDRESS(ES)
Naval Postgraduate School
Monterey CA 93943-5000

8. PERFORMING ORGANIZATION REPORT NUMBER

9. SPONSORING/MONITORING AGENCY NAME(S) AND ADDRESS(ES)

10. SPONSORING/MONITORING AGENCY REPORT NUMBER

11. SUPPLEMENTARY NOTES The views expressed in this thesis are those of the author and do not reflect the official policy or position of the Department of Defense or the U.S. Government.

12a. DISTRIBUTION/AVAILABILITY STATEMENT
Approved for public release; distribution is unlimited.

12b. DISTRIBUTION CODE
A

13. ABSTRACT *(maximum 200 words)*

A new method is presented for estimating the reflection of a random, multi-directional sea from a coastal structure. The technique is applicable to an array of wave gauges of arbitrary geometry deployed seaward of the reflector. An expansion for small oblique wave incidence angles is used to derive an approximate relationship between measured array cross-spectra and a small number of parameters that describe the incident wave properties and the reflectivity of the structure. Model tests with simulated array data demonstrate that for wave incidence angles less than about 30° the new technique provides accurate and robust estimates of the gross properties of incident and reflected waves.

The new method is applied to array data acquired offshore of a permeable, rubble mound breakwater in Monterey Bay, California. The estimated reflection coefficients decrease approximately linearly with increasing frequency. Whereas the observed reflections depend only weakly on the incident wave energy, the fraction of the incident wave energy flux transmitted through the breakwater decreases with increasing wave energy, suggesting that dissipation is enhanced with large amplitude waves.

14. SUBJECT TERMS Reflections, Waves, Breakwater			15. NUMBER OF PAGES 47
			16. PRICE CODE
17. SECURITY CLASSIFICATION OF REPORT Unclassified	18. SECURITY CLASSIFICATION OF THIS PAGE Unclassified	19. SECURITY CLASSIFICATION OF ABSTRACT Unclassified	20. LIMITATION OF ABSTRACT UL

NSN 7540-01-280-5500

Standard Form 298 (Rev. 2-89)
Prescribed by ANSI Std. 239-18

Approved for public release; distribution is unlimited.

Wave Reflections from Breakwaters

by

William S. Dickson
Lieutenant, United States Navy
B.S., United States Naval Academy, 1988

Submitted in partial fulfillment
of the requirements for the degree of

MASTER OF SCIENCE IN (Meteorology and Physical Oceanography)

from the

NAVAL POSTGRADUATE SCHOOL
June 1994

Author: 

William S. Dickson

Approved by: 

T. H. C. Herbers, Thesis Advisor

E. B. Thornton, Co-Advisor

C. A. Collins, Chairman
Department of Oceanography

TABLE OF CONTENTS

LIST OF SYMBOLS

η_i, η_r=surface elevation functions of incident and reflected waves

$\mathbf{k}, \mathbf{k}_r$=vector wavenumbers of incident and reflected waves

dz=incident wave amplitude

$\mathbf{x}$=horizontal position vector

t=time

ω=radian frequency

R=reflection coefficient

ϕ=phase lag between incident and reflected waves

h_{nm}=cross-spectrum of sensors m and n

τ=time lag

E{}=expected value

g=gravity

h=water depth

θ=wave incidence angle

x,y=horizontal position coordinates

k=wavenumber

R_0, ϕ_0, R_2, ϕ_2=reflection parameters

L=distance from coordinate origin to the breakwater

E=incident wave energy spectral density

θ_{mean}=mean propagation direction of incident waves

θ_{rms}=root-mean-square directional spread of incident waves

$\hat{E}$, $\hat{\theta}_{mean}$, $\hat{R}_0$, $\hat{\phi}_0$=estimates of incident and reflected wave parameters

$\tilde{h}_{nm}$, $\hat{h}_{nm}$=observed and model cross-spectra

ε=root-mean-square misfit norm

$\bar{E}$=average of the auto-spectra

f=frequency (Hz)

F_i=incident energy flux density

F_r=reflected energy flux density

F_t=transmitted energy flux density

F_d=dissipated energy flux density

Cg_1, Cg_2=group velocity outside and inside the harbor

T=transmission coefficient

ACKNOWLEDGMENTS

This research was funded by the U. S. Army Corps of Engineers, District Office San Francisco and the Office of Naval Research, Coastal Sciences Program. The pressure sensor array was deployed by a student officer, SEAL dive team led by Tom Schmottlach. And, it was maintained by the staff of the Naval Postgraduate School, Department of Oceanography along with a UDT dive team from Treasure Island, Ca, who also retrieved the array.

I. INTRODUCTION

The interaction of ocean surface waves with a permeable, rubble mound breakwater is complex. In general, the incident waves are partially transmitted through or over the porous structure, partially dissipated by breaking on the rough slopes and by turbulent friction within the breakwater, and partially reflected. The reflection of waves from breakwaters (and other reflectors such as sand bars and seawalls) is usually measured with an array of pressure sensors or surface height gauges deployed seaward of the reflector (e.g., Thornton and Calhoun 1972; Mansard and Funke 1980; Yokoki et al. 1992). The interpretation of these measurements is complicated owing to the fact that the incident and reflected waves are phase-coupled.

In many studies the array analysis is simplified by assuming that the incident waves are uni-directional, propagating perpendicular to the reflector. Thornton and Calhoun (1972), Morden et al. (1976) and Goda and Suzuki (1976) used two sensors positioned on a line perpendicular to the reflector to decompose the wave field into incident and reflected wave contributions. This technique breaks down at the frequency where the wavelength is equal to twice the sensor spacing. Mansard and Funke (1980) overcame this problem by applying a least-squares-fit technique to three

sensors, and this approach was extended to linear arrays with an arbitrary number of sensors by Zelt and Skjelbreia (1992).

The assumption of normally incident waves used to estimate reflection is often violated in a natural coastal environment. Refraction of swell over complex bathymetry may result in significantly oblique angles of incidence at the breakwater, especially if the breakwater is not aligned with the surrounding depth contours. Directionally broad, locally generated seas are typically only weakly refracted in depths greater than 10 m and can approach a breakwater at relatively large oblique angles. Although in principal array measurements seaward of a reflector can be used to infer the reflection of a directionally spread wave field, a very large number of sensors is required to obtain reliable estimates of the directional spectra of both incident and reflected waves (Isobe and Kondo 1984).

In this study, a new method is presented for estimating wave reflections from array data. The assumption of normal incidence used in previous studies is relaxed, but angles of incidence are assumed to be small. Reflection from the breakwater is assumed to be a linear process governed by Snell's law (i.e., specular reflection). An expansion for small oblique incidence angles is used to derive approximate relationships between the array cross-spectra and a small

number of parameters that describe the incident wave properties and the reflectivity of the breakwater.

The new estimating technique is applied to pressure array data acquired offshore of the Monterey Harbor breakwater at Monterey, California. The field site, array geometry and data acquisition are described in Section 2. Section 3 presents the new estimation technique, and demonstrates the accuracy and robustness of the method through model simulations. Results of the analysis of reflections observed at the Monterey breakwater are given in Section 4, followed by a discussion and conclusions in Section 5.

II. EXPERIMENT

The experiment was conducted at the Monterey Harbor breakwater in Monterey, California (Fig. 1). Situated at the southern end of Monterey Bay (Fig. 1a), the permeable breakwater is exposed only to swell with deep water propagation directions ranging from west to north-northwest and seas generated by local northerly winds. The (refracted) directional wave spectra at this sheltered site are typically narrow with most of the energy approaching the breakwater from northerly directions within about 20° of normal incidence to the breakwater.

Construction of the 400 m long rubble mound breakwater was completed in 1934, and that same year a 120 m long extension was added (Fig. 1b). During subsequent years, much of the interior of the breakwater washed away and the elevation of the structure decreased so that it was often overtopped at high tide (Thornton and Calhoun 1972). In 1993, the breakwater extension was improved by increasing the elevation back to the original design height of +3 m relative to MLLW, and by adding on the harbor side a single cover layer of 8-ton-average armor stone. A cross section of the breakwater can be found in Thornton and Calhoun (1972). The present field study was conducted at the improved extension.

A 2-dimensional array of six pressure sensors was deployed seaward of the breakwater in a depth of about 16 m (Fig. 1b) to measure both the incident and reflected wave fields. The small depth variations (less than 1.5 m) across the array are neglected. The array aperture is 31 m x 15.6 m and the distance between the breakwater and the closest sensor P6 is about 52 m. Additionally, a single pressure sensor P7 was positioned inside the harbor at a distance of about 47 m from the breakwater to measure the transmitted wave field. Sensor locations relatively close to the breakwater were chosen to avoid contamination by edge effects (e.g., diffraction around the tip of the breakwater).

The array data were acquired with a tattletail microprocessor located in the center of the array, which was cabled to a radiotelemetry system on the breakwater, from where the data were transmitted to a computer at the Naval Postgraduate School. Data were acquired with a 2 Hz sample rate continuously for eight months between August 1993 and March 1994.

Typical power spectra measured along a line perpendicular to the breakwater, converted to surface height with a linear theory depth correction, are shown in Fig. 2. The swell spectrum is most energetic in the frequency range of about 0.06-0.1 Hz. Large differences in energy levels

is the vector wavenumber of the reflected wave. R, ϕ and $\mathbf{k}_r$ are generally functions of $\mathbf{k}$ and ω. Adding Eqs. 1 and 2 yields the total surface elevation function $\eta(\mathbf{x},t)$:

$$\eta(\boldsymbol{x},t) = \int_{\omega}\int_{\boldsymbol{k}}[\exp[i(\boldsymbol{k}\cdot\boldsymbol{x}-\omega t)] + R\exp[i(\boldsymbol{k}_r\cdot\boldsymbol{x}-\omega t+\phi)]]\,dz(\omega,\boldsymbol{k}) \tag{3}$$

The cross-spectrum $h_{nm}(\omega)$ of two sensors at positions $\mathbf{x}_m$ and $\mathbf{x}_n$ is defined as:

$$\int_{\omega}\exp[i\omega\tau]\,h_{nm}(\omega)\,d\omega \equiv E\{\eta(\boldsymbol{x}_m,t)\,\eta^*(\boldsymbol{x}_n,t+\tau)\} \tag{4}$$

where E{} denotes the expected value and * the complex conjugate. Substitution of Eq. 3 in Eq. 4 yields:

$$h_{nm}(\omega) = \int_{\boldsymbol{k}}[\exp[i\boldsymbol{k}\cdot\boldsymbol{x}_m] + R\exp[i(\boldsymbol{k}_r\cdot\boldsymbol{x}_m+\phi)]] \times [\exp[-i\boldsymbol{k}\cdot\boldsymbol{x}_n] + R\exp[-i(\boldsymbol{k}_r\cdot\boldsymbol{x}_n+\phi)]]S(\omega,\boldsymbol{k})\,d\boldsymbol{k} \tag{5}$$

where $S(\omega,\mathbf{k})$ is the wavenumber-frequency spectrum:

$$S(\omega,\boldsymbol{k}) = \frac{E\{dz(\omega,\boldsymbol{k})\,dz^*(\omega,\boldsymbol{k})\}}{d\omega\,d\boldsymbol{k}} \tag{6}$$

The wavenumber magnitudes of both incident and reflected waves are given by the linear dispersion relation $\omega^2=gk[\tanh(kh)]$, where $k=|\mathbf{k}|=|\mathbf{k}_r|$, g is gravity and h the water depth. Introducing polar coordinates ($\mathbf{k}=[k(\cos(\theta)),k(\sin(\theta))]$) and further assuming that the reflection is specular ($\mathbf{k}_r=[-k(\cos(\theta)),k(\sin(\theta))]$), Eq. 5

can be expressed as (dropping the frequency dependence):

$$h_{nm} = \int_{-\frac{\pi}{2}}^{\frac{\pi}{2}} G_{nm}(\theta)\, S(\theta)\, d\theta \tag{7}$$

where $G_{nm}(\theta)$ is given by:

$$\begin{aligned} G_{nm}(\theta) = & [\exp[ik(x_m\cos\theta + y_m\sin\theta)] \\ & + R(\theta)\exp[i(-kx_m\cos\theta + ky_m\sin\theta + \phi(\theta))]] \\ & \times [\exp[-ik(x_n\cos\theta + y_n\sin\theta)] \\ & + R(\theta)\exp[-i(-kx_n\cos\theta + ky_n\sin\theta + \phi(\theta))]] \end{aligned} \tag{8}$$

and $S(\theta)$ is the directional spectrum of incident waves.

Assuming that incident waves approach the breakwater at small oblique angles, R and ϕ can be expanded for small θ:

$$R(\theta) = R_0 + R_2\theta^2 + R_4\theta^4 + \ldots \tag{9}$$

$$\phi(\theta) = \phi_0 + \phi_2\theta^2 + \phi_4\theta^4 + \ldots \tag{10}$$

The odd-order terms in these expansions vanish because $R(\theta)$ and $\phi(\theta)$ are symmetric functions. Substituting Eqs. 9 and 10 in Eq. 8 and expanding $G_{nm}(\theta)$ for small θ yields :

$$G_{nm}(\theta) = A_{nm} + B_{nm}\theta + C_{nm}\theta^2 + D_{nm}\theta^3 + \ldots \tag{11}$$

with the lowest three coefficients A_{nm}, B_{nm} and C_{nm} given by:

$$\begin{aligned} A_{nm} = & \exp[ik(x_m - x_n)] + 2R_0\cos[k(x_m + x_n) - \phi_0] \\ & + R_0^2\exp[-ik(x_m - x_n)] \end{aligned} \tag{12a}$$

$$B_{nm}=ik(y_m-y_n)A_{nm} \tag{12b}$$

$$\begin{aligned} C_{nm}=&-\frac{1}{2}(k^2(y_m-y_n)^2+ik(x_m-x_n))\exp[ik(x_m-x_n)] \\ &+[2R_2-R_0k^2(y_m-y_n)^2]\cos(k(x_m+x_n)-\phi_0) \\ &+[2R_0\phi_2+R_0k(x_m+x_n)]\sin(k(x_m+x_n)-\phi_0) \\ &+[\frac{1}{2}R_0^2(-k^2(y_m-y_n)^2+ik(x_m-x_n))+2R_0R_2]\exp[-ik(x_m-x_n)] \end{aligned} \tag{12c}$$

$G_{nm}(\theta)$ can be accurately approximated by a truncated expansion of the form Eq. 11 if all the expansion coefficients (Eq. 12) are $\leq O(1)$. Thus the technique presented here is generally valid only for compact arrays (i.e., $|\mathbf{k}\cdot\mathbf{x}|\leq O(1)$) positioned close to the reflector (i.e., within a wavelength so that $\phi\leq O(1)$).

The exact $G_{nm}(\theta)$ (Eq. 8) of sensor pair n=3, m=1 (Fig. 1b) for $f=\frac{\omega}{2\pi}=.08$ Hz (the dominant swell frequency) is compared to the linear $(A_{nm}+B_{nm}\theta)$ and quadratic $(A_{nm}+B_{nm}\theta+C_{nm}\theta^2)$ approximations in Fig. 3. In this calculation the breakwater is idealized as a partially absorbing wall at x=L=83 m with R independent of θ and $\phi=2kL[\cos(\theta)]$ (Fig. 1b). The linear approximation diverges from the exact solution for $|\theta|>5$-$15°$ but errors are generally within 10% even for incidence angles as large as 30°. The quadratic approximation is more accurate for small values of θ, but diverges sharply from the exact solution for large θ with

deviations exceeding 20% for $|\theta| \geq 30°$. Similar calculations for other sensor pairs and other frequencies in the swell range (0.05-0.12 Hz) show comparable agreement between the exact $G_{nm}(\theta)$ and the linear and quadratic approximations.

Substitution of the truncated expansion of $G_{nm}(\theta)$ (Eqs. 11,12) in Eq. 7 yields the quadratic approximation of the cross-spectrum h_{nm}:

$$h_{nm} \approx A_{nm}(R_0, \phi_0)\, E + B_{nm}(R_0, \phi_0)\, \theta_{mean} E + C_{nm}(R_0, R_2, \phi_0, \phi_2)\, [\theta^2_{rms} + \theta^2_{mean}]\, E \tag{13}$$

where E, θ_{mean} and θ_{rms} are the energy spectral density (integrated over all directions), mean propagation direction and root-mean-square directional spread of the incident waves:

$$E = \int_{-\frac{\pi}{2}}^{\frac{\pi}{2}} S(\theta)\, d\theta \tag{14a}$$

$$\theta_{mean} = \frac{\int_{-\frac{\pi}{2}}^{\frac{\pi}{2}} \theta S(\theta)\, d\theta}{\int_{-\frac{\pi}{2}}^{\frac{\pi}{2}} S(\theta)\, d\theta} \tag{14b}$$

$$\theta_{rms} = \left[\frac{\int_{-\frac{\pi}{2}}^{\frac{\pi}{2}} (\theta - \theta_{mean})^2 S(\theta)\, d\theta}{\int_{-\frac{\pi}{2}}^{\frac{\pi}{2}} S(\theta)\, d\theta} \right]^{\frac{1}{2}} \tag{14c}$$

Eq. 13 relates the array cross-spectra h_{nm} to three parameters of the incident wave field (E, θ_{mean}, θ_{rms}) and four reflection parameters (R_0 , ϕ_0 , R_2 , ϕ_2). In general, inverse algorithms can be developed that search for a combination of these seven parameters on a frequency by frequency band basis such that the associated cross-spectra are as close as possible to the observed cross-spectra, but this requires an extensive array. Since the six-element array deployed in the present study is relatively small in aperture, the contributions of the quadratic (C_{nm}) terms to Eq. 13 is small even for wave incidence angles as large as 20° (e.g., compare the linear and quadratic approximations of $G_{31}(\theta)$ in Fig. 3). Thus, the higher-order parameters θ_{rms}, R_2, and ϕ_2 may not be resolvable within the uncertainty of the array cross-spectra. Neglecting the quadratic terms in Eq. 13 reduces the inverse problem to only four unknowns: two incident wave parameters (E, θ_{mean}) and two reflection parameters (R_0 , ϕ_0). Estimates $\hat{E}$, $\hat{\theta}_{mean}$, $\hat{R}_0$ and $\hat{\phi}_0$ were obtained by minimizing a simple root-mean-square misfit norm ε:

$$\epsilon = \left(\frac{\sum_n \sum_m (\hat{h}_{nm} - \tilde{h}_{nm})\,(\hat{h}^*_{nm} - \tilde{h}^*_{nm})}{\sum_n \sum_m \tilde{h}_{nm} \tilde{h}^*_{nm}} \right)^{\frac{1}{2}} \qquad (15)$$

with $\tilde{h}_{nm}$ the observed cross-spectra and $\hat{h}_{nm}$ the linear model

$$\hat{h}_{nm}=A_{nm}(\hat{R}_0,\hat{\phi}_0)\,\hat{E}+B_{nm}(\hat{R}_0,\hat{\phi}_0)\,\theta_{mean}\hat{E} \qquad (16)$$

Since both the number of sensors and the number of unknowns is small, this minimum misfit can be evaluated by essentially sweeping through the entire parameter space. For all possible combinations of $\hat{E}$, $\hat{\theta}_{mean}$, $\hat{R}_0$ and $\hat{\phi}_0$, the cross-spectra $\hat{h}_{nm}$ and the misfit ε were calculated with Eqs. 12a, b, 15 and 16 to obtain a global minimum for ε. The range of physically plausible values for $\hat{E}$, $\hat{\theta}_{mean}$, $\hat{R}_0$ and $\hat{\phi}_0$ used in these calculations is $0.25\bar{E}$-$4\bar{E}$, -30°-30°, 0-1, and 0-360°, respectively, with $\bar{E}$ the average of the auto spectra $\tilde{h}_{nn}$. The minimum value of ε was calculated by sweeping through all possible combinations of E, θ_{mean}, R_0, ϕ_0, stepping with increments of $0.15\bar{E}$, 5°, 0.1, and 15°, that were somewhat coarse owing to limited computing resources. The accuracy of the solution $\hat{E}$, $\hat{\theta}_{mean}$, $\hat{R}_0$, $\hat{\phi}_0$ was improved by sweeping with smaller step sizes ($0.03\bar{E}$, 2°, 0.02, 3°) through a reduced parameter range ($\hat{E}\pm0.3\bar{E}$, $\hat{\theta}_{mean}\pm10°$, $\hat{R}_0\pm0.2$, $\hat{\phi}_0\pm30°$).

The accuracy of the new estimation technique was verified through a series of model tests with simulated array cross-spectra. For a chosen incident swell

directional spectrum of the form:

$$S(\theta) \propto \cos^{200}\left(\frac{\theta-\theta_{mean}}{2}\right)$$

the true cross-spectra h_{nm} of the Monterey array (Fig. 1b) were evaluated with Eqs. 7 and 8. As before, the breakwater was idealized in these tests as a partially absorbing wall at x=L=83 m with R independent of θ and $\phi=2kL[\cos(\theta)]$. In each test, five random realizations of cross-spectra $\tilde{h}_{nm}$ were generated using the procedure described in Long and Hasselmann (1979). Errors in the simulated $\tilde{h}_{nm}$ include both statistical uncertainty resulting from finite length data records (160 degrees of freedom) and uncorrelated instrument noise (noise to signal ratio 0.05) and are roughly representative of the actual array measurements presented in Section 4. The simulated $\tilde{h}_{nm}$ were then treated in exactly the same way as cross-spectra obtained from ocean observations, and the minimum misfit ε and the optimal parameters $\hat{E}$, $\hat{\theta}_{mean}$, $\hat{R}_0$, $\hat{\phi}_0$, were obtained with the inverse algorithm described above.

Results of model tests for typical swell with frequency f=0.086 Hz are presented in Figs. 4 and 5. Similar comparisons (not shown) for other frequencies in the swell band (0.05-0.12 Hz) yielded comparable agreement. Estimated ($\hat{R}$) and true (R) reflection coefficients are in good

agreement for both normally (Fig. 4a) and obliquely (Fig. 4b) incident swell (discrepancies generally within ±0.05). Estimates of the incident wave energy E (Fig. 4c) and propagation direction θ_{mean} (Fig. 5) also agree well with the input spectrum (errors generally less than 20% and 4°, respectively). The values of the misfit ε, a normalized rms measure of the discrepancies between the model ($\hat{h}_{nm}$) and "observed" ($\tilde{h}_{nm}$) cross-spectra (Eq. 15), range from 0.02 to 0.08 (Fig. 4d). The misfits are generally larger for the simulations with obliquely propagating waves than for normally incident waves (e.g., compare the ε for θ_{mean}=0° and 20° in Fig. 4d) owing to errors in $\hat{h}_{nm}$ based on a small θ approximation (Eq. 16). However, aside from a slight bias in $\hat{R}$ (Fig. 4b), the estimates of incident and reflected wave parameters do not appear to be significantly degraded for θ_{mean}=20° (Figs. 4,5).

Overall, the model simulations demonstrate that the estimation technique is relatively insensitive to errors in the data and the model, and can extract accurate estimates of wave reflections from the array data acquired in the present study.

IV. OBSERVED REFLECTIONS

The reflection estimation technique described in the previous section was applied to the array measurements acquired at the Monterey Harbor breakwater (Fig. 1). Nine days were selected for analysis, that approximately span the range of conditions encountered during the experiment. For each of these nine days, two three hour data runs were processed, one acquired at low tide and one at high tide, with the objective to examine the sea level dependence of breakwater reflections. Cross-spectra with a frequency resolution of 0.0078 Hz and 160 degrees of freedom were computed for each of the 18 data runs. For every frequency band in the dominant swell range, 0.05 Hz-0.12 Hz, the inverse algorithm was applied to the cross-spectra to estimate the incident wave spectral density E(f), the mean incident wave propagation direction $\theta_{mean}(f)$, the reflection coefficient $R_0(f)$ and the phase lag between incident and reflected waves $\phi_0(f)$. Frequencies less than 0.05 Hz and greater than 0.12 Hz are not considered here because infragravity waves dominate the spectra below 0.05 Hz (e.g., Fig. 2; Okihiro et al. 1992) and above 0.12 Hz (i.e., frequencies greater than about twice the spectral peak frequency) local nonlinear effects may be significant.

The variability of incident wave conditions was small. Estimates of the incident swell variance ranged from 3.7 cm^2 to 51 cm^2 (i.e., significant wave heights of 7-29 cm). These low energy conditions are typical for this site owing to sheltering effects (Fig. 1), and the fact that no major storm occurred during the eight month data acquisition period. Estimates of the mean frequency and propagation direction of incident waves (averages of f and $\theta_{mean}(f)$ over the swell band, weighted by E(f)) ranged from 0.065-0.089 Hz and from 0-18°. These incidence angles are well within the range for which the present technique (based on a small θ expansion) is expected to be accurate (Figs. 3-5).

Estimates of $R_0(f)$ obtained from different data runs are remarkably similar (Fig. 6), even though the incident wave spectral levels varied by more than an order of magnitude. Reflection of small amplitude swell from the breakwater is apparently insensitive to the incident wave amplitude, consistent with the assumption that reflection is a linear process. In all cases the reflection estimates show a strong frequency dependence with $\hat{R}_0(f)$ decreasing approximately linearly with increasing frequency from about 0.7-0.8 for f=0.05 Hz to 0.2-0.3 for f=0.12 Hz. In contrast to estimates reported by Thornton and Calhoun (1972), the present observations do not suggest a strong dependence of R on tidal sea level variations.

The misfit ε between $\tilde{h}_{nm}$ and $\hat{h}_{nm}$ (Eq. 15) is shown in Fig. 7 as a function of frequency. In the most energetic part of the spectrum (0.06-0.1 Hz), ε is approximately 0.03-0.07, comparable to the misfits obtained in model tests. At frequencies below 0.06 Hz and above 0.1 Hz, where energy levels are relatively low, the misfits are slightly larger (0.05-0.16) than expected from model tests, possibly owing to directional spreading and/or nonlinear effects.

Estimates of the phase lag $\phi_0(f)$ between incident and reflected waves obtained from 18 different data runs are approximately equal, increasing with increasing frequency as expected from theory (Fig. 8). Neglecting depth variations (i.e., changes in k) seaward of the breakwater, the theoretical phase lag ϕ_0 for small incidence angles is equal to 2kL. This crude approximation of ϕ_0, taking L to be the distance to the crest of the breakwater, is in good agreement with the estimates across the entire swell band (Fig. 8).

V. DISCUSSION AND CONCLUSIONS

A single sensor (P7) was deployed inside the harbor (Fig. 1b) to obtain crude estimates of wave transmission through the breakwater. Assuming that the propagation directions of incident, reflected and transmitted waves are nearly perpendicular to the breakwater, the fluxes of incident ($F_i(f)$), reflected ($F_r(f)$) and transmitted ($F_t(f)$) energy are approximately given by:

$$F_i(f) = E(f)\, Cg_1(f) \tag{17a}$$

$$F_r(f) = R^2(f)\, E(f)\, Cg_1(f) \tag{17b}$$

$$F_t(f) = E_{P7}(f)\, Cg_2(f) \tag{17c}$$

where Cg_1 and Cg_2 are the group velocities at the offshore array and sensor P7, E is the estimated incident wave spectrum and E_{P7} is the transmitted wave spectrum measured by sensor P7. The transmission coefficient T(f), defined as:

$$T = \sqrt{\frac{F_t(f)}{F_i(f)}} \tag{18}$$

is plotted as a function of frequency in Fig. 9 for all 18 data runs. The observed transmission coefficients are more variable than the reflection coefficients (Fig. 6), but do not suggest a consistent sea level or frequency dependence.

Estimates of the residual energy flux F_d :

$$F_d(f) = F_i(f) - F_r(f) - F_t(f) \qquad (19)$$

that is dissipated through wave breaking on the rough breakwater slope and/or turbulent friction inside the porous structure, are variable, but F_d/F_i generally increases with increasing frequency (Fig. 10).

Estimates of the bulk incident, reflected, transmitted and dissipated energy fluxes, obtained by integrating $F_i(f)$, $F_r(f)$, $F_t(f)$ and $F_d(f)$ over the entire swell band (0.05-0.12 Hz), are presented in Fig. 11. The observed fraction of the incident energy flux that is reflected from the breakwater (Fig. 11a) varies between about .2 and .5. These changes in the breakwater reflectivity are primarily the result of variations in the dominant swell frequency (0.06-0.09 Hz, Fig. 6). On the other hand transmission of wave energy through the breakwater appears to be a strong function of the incident energy flux (Fig. 11b). On days with very low amplitude swell about 40-60% of the incident energy flux is transmitted through the breakwater and dissipation is weak (0-40%, Fig. 11c). On more energetic days about 40-60% of the incident energy flux is dissipated (Fig. 11c) and the transmission is reduced to about 20-30% of the incident energy flux (Fig. 11b).

Estimates of energy transmission and dissipation also show a dependence on sea level. At high tide the

transmitted (dissipated) energy fluxes are slightly larger (smaller) than at low tide, possibly owing to the fact that the effective width of the breakwater near the sea surface is smaller at high tide than at low tide.

Waves transmitted through the breakwater may undergo partial reflection at the other side of the harbor and the associated standing wave patterns may contribute significant errors to estimates of $F_t(f)$ based on Eq. 17c. Accurate estimation of wave transmission requires an array of sensors on the harbor side of the breakwater, which was not available in this study. Furthermore, the range of conditions encountered in the present experiment was rather limited, and the reflection/transmission coefficients observed under benign conditions may not be representative for the breakwater performance under storm or large amplitude swell conditions. More extensive measurements are needed to evaluate the performance of permeable rubble mound breakwaters.

The main result of the present study is the development of a new technique for estimating the reflection of a random, directionally spread wave field from a coastal structure (e.g., a breakwater or seawall) or natural sand bars. The estimation technique can be applied to a compact (i.e., aperture less than a wavelength) array of pressure sensors or surface height gauges of arbitrary geometry,

deployed seaward of the reflecting surface (within a wavelength). Model tests demonstrate that for wave incidence angles less than about 30° the new method can provide accurate estimates of the gross properties of incident and reflected waves.

APPENDIX

Figure 1. a) Location of the Monterey Harbor breakwater. b) Coordinate frame and locations of pressure sensors deployed near the 120 m breakwater extension. The three sensors in the center (P2,P4,P5) form an equilateral triangle with dimension 2.5 m. P1 is 15 m seaward of the triangle, P3 and P6 are both positioned at a distance of 13 m from the center. Sensor P7 is inside the harbor. Soundings are in meters relative to MLLW.

Figure 2. Typical power spectra of array sensors P1 (solid), P5 (dashed), P6 (dotted), positioned on a line perpendicular to the breakwater (Fig. 1b). The dash-dot curve is the spectrum measured inside the harbor (sensor P7).

Figure 3. The exact $G_{nm}(\theta)$ (solid lines, Eq. 8) compared to quadratic (left panels) and linear (right panels) approximations (dashed lines, Eq. 11), for sensor pair n=3, m=1, with the reflection coefficient, R, equal to 0, .5 and 1.

Figure 4. Results of model tests for normally ($\theta_{mean}=0°$) and obliquely ($\theta_{mean}=20°$) incident waves, with the reflection coefficient, R_0, varying from 0 to 1. a) $\hat{R}_0$ vs R_0 for $\theta_{mean}=0°$. b) $\hat{R}_0$ vs R_0 for $\theta_{mean}=20°$. c) Ratio between estimated ($\hat{E}$) and true (E) incident wave energy vs R_0. d)

between the estimates and true values. Pluses and circles in panels c) and d) correspond to θ_{mean}=0° and 20° simulations.

Figure 5. Results of a model test for a reflection coefficient R_0=.5 and mean incidence angles θ_{mean} varying from 0°-20°. The estimated incidence angle $\hat{\theta}_{mean}$ is compared to θ_{mean}. The solid line denotes perfect agreement.

Figure 6. Estimated reflection coefficient $\hat{R}_0$ vs. frequency for all 18 data runs. The solid and dashed lines indicate low and high tide runs.

Figure 7. Misfit ε between $\tilde{h}_{nm}$ and $\hat{h}_{nm}$ as a function of frequency for all 18 data runs. The solid and dashed lines indicate low and high tide runs.

Figure 8. The estimated phase lag $\hat{\phi}_0$ between incident and reflected waves (relative to x=0) as a function of frequency for all 18 data runs. Circles and crosses indicate low and high tide runs. The solid line is a crude theoretical approximation of ϕ_0.

Figure 9. The transmission coefficient T as a function of frequency for all 18 data runs. The solid and dashed lines indicate low and high tide runs.

Figure 10. The ratio of dissipated to incident energy flux as a function of frequency for all 18 data runs. The solid and dashed lines indicate low and high tide runs.

Figure 11. The ratios of reflected to incident (a), transmitted to incident (b), and dissipated to incident (c)

Figure 11. The ratios of reflected to incident (a), transmitted to incident (b), and dissipated to incident (c) energy fluxes vs. the incident energy flux for all 18 data runs. The energy fluxes are integrated across the swell band (0.05-0.12). The circles and crosses represent low and high tide runs.

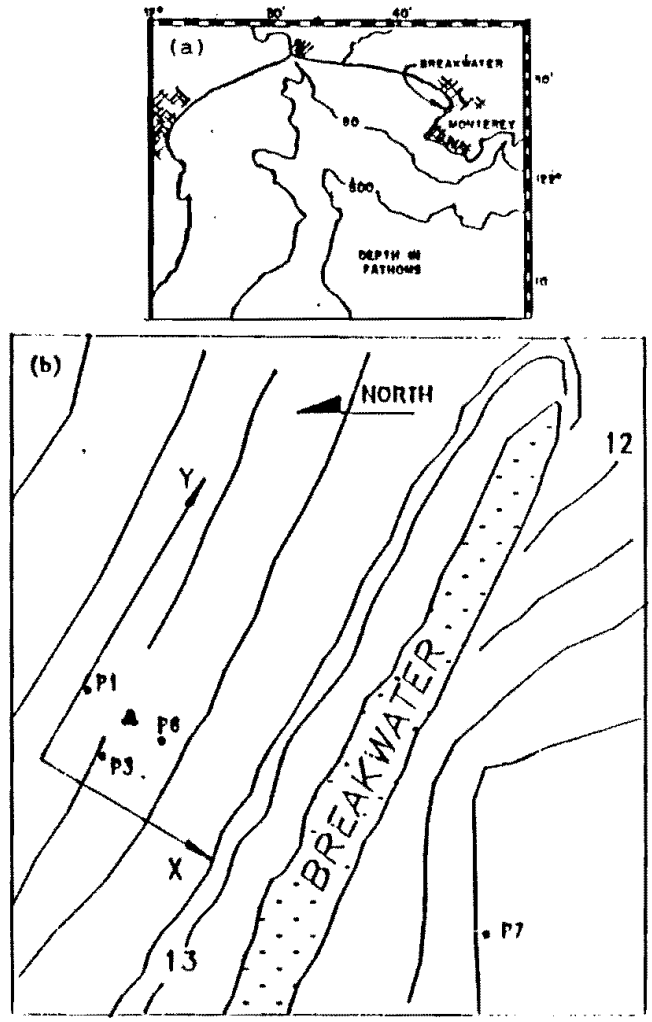
(a)
BREAKWATER
MONTEREY
DEPTH IN FATHOMS
(b)
NORTH
Y
X
P1
P6
P3
P7
12
13
BREAKWATER

Figure 1.

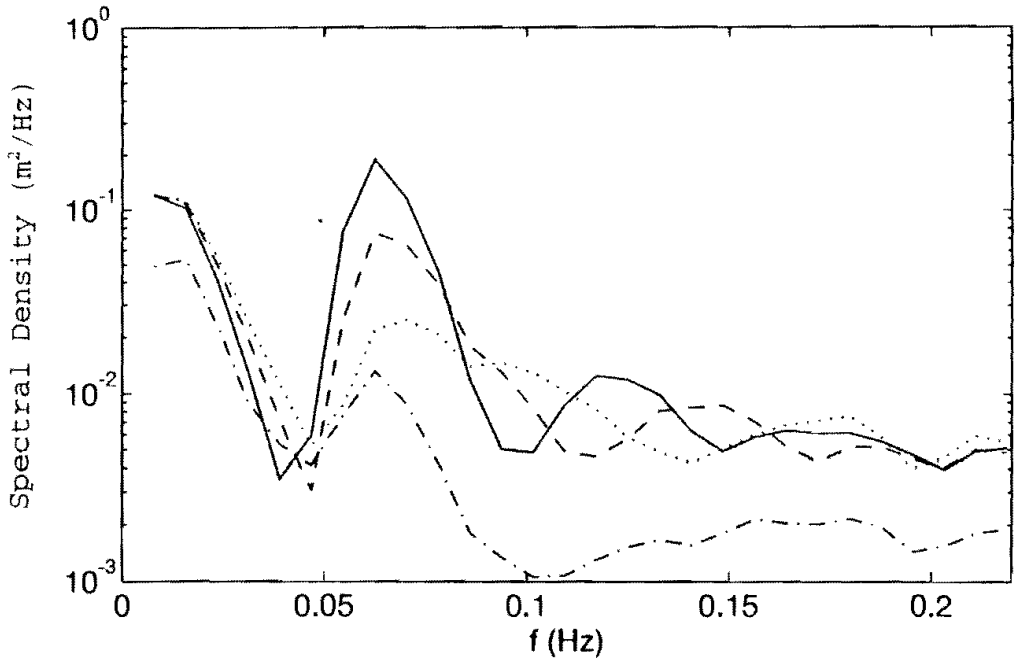

Figure 2.

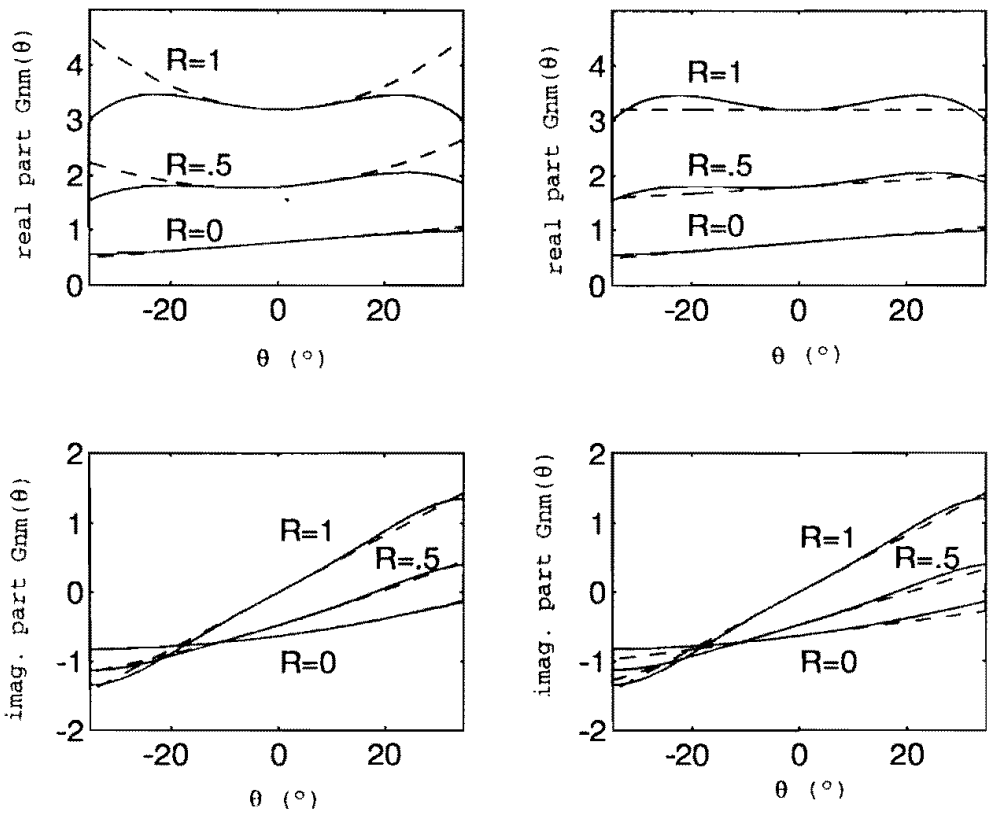

Figure 3.

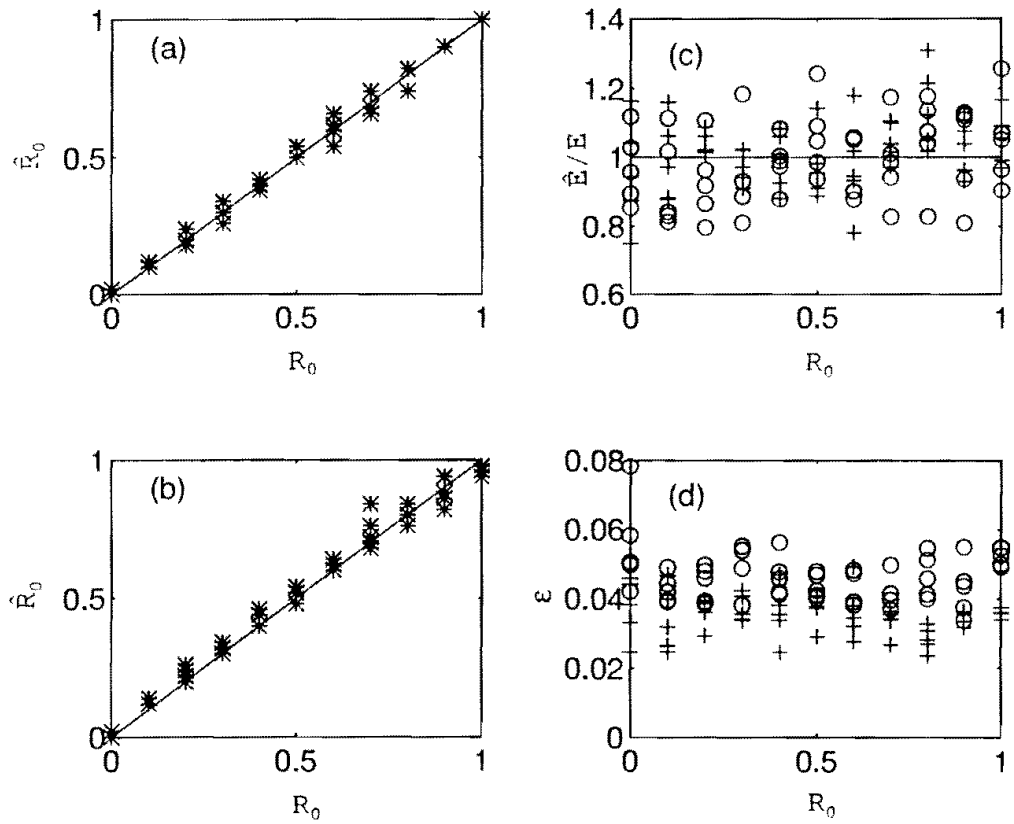
(a)
(b)
(c)
(d)
$\hat{R}_0$
R_0
$\hat{E}/E$
ε
0
0.5
1
0.6
0.8
1.2
1.4
0.02
0.04
0.06
0.08

Figure 4.

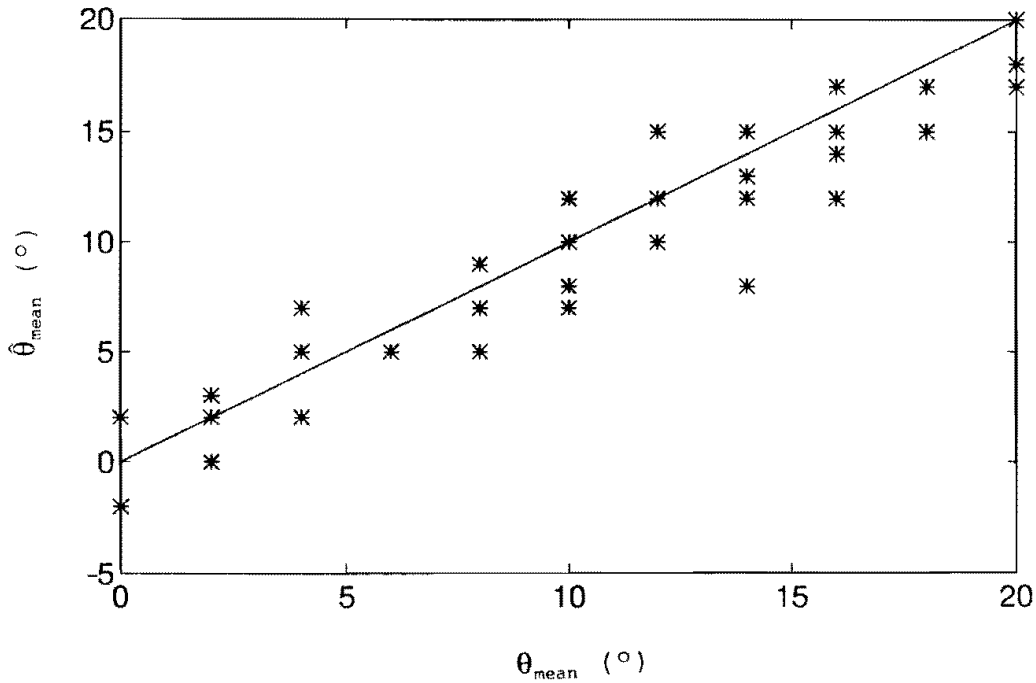

Figure 5.

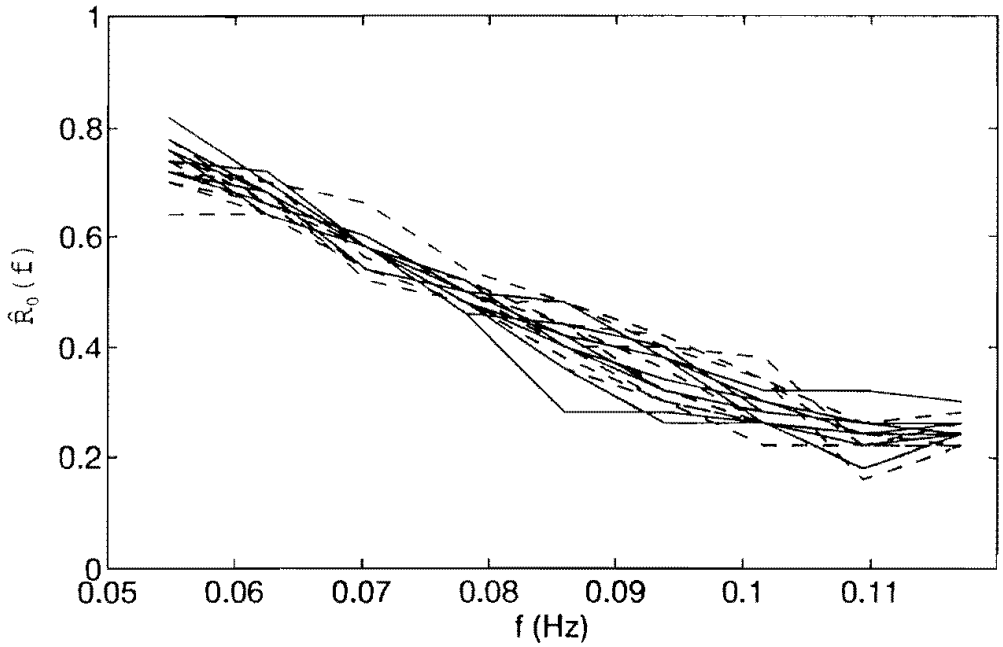

Figure 6.

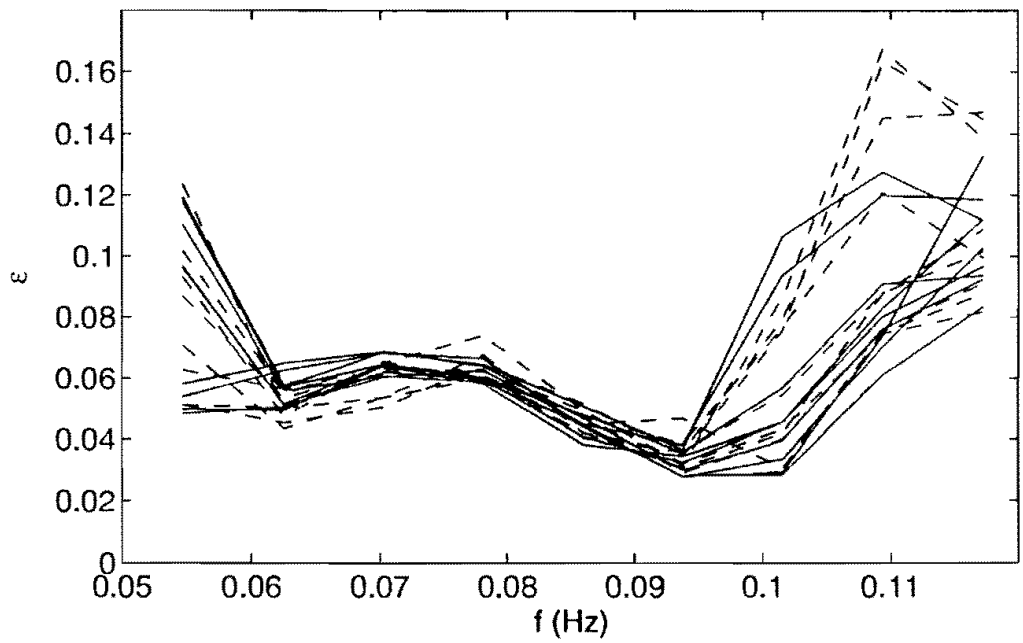

Figure 7.

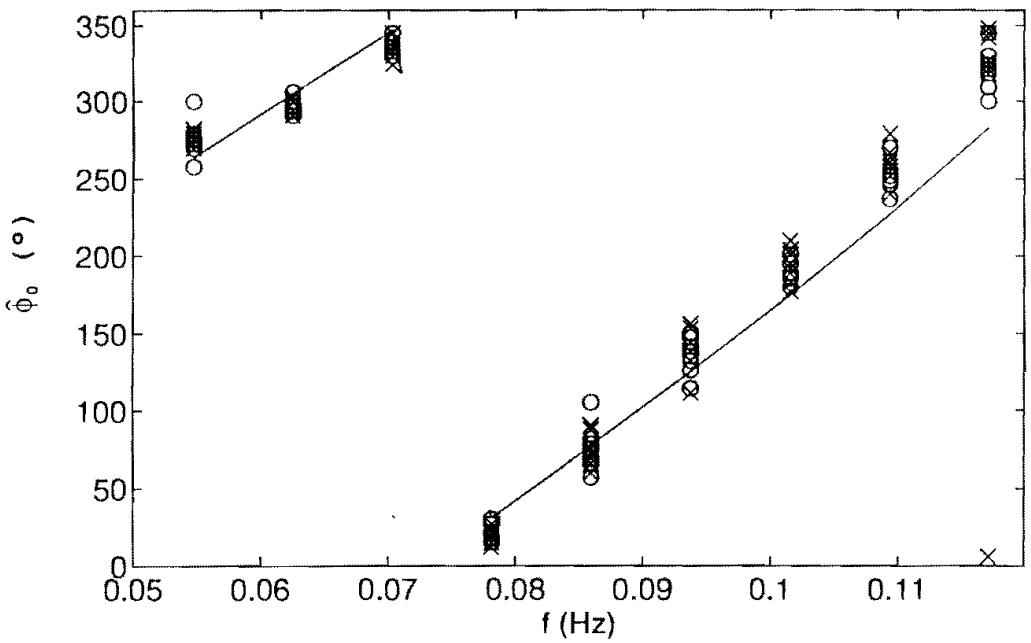
350
300
250
200
150
100
50
0
0.05
0.06
0.07
0.08
0.09
0.1
0.11
f (Hz)
$\hat{\phi}_0$ (°)

Figure 8.

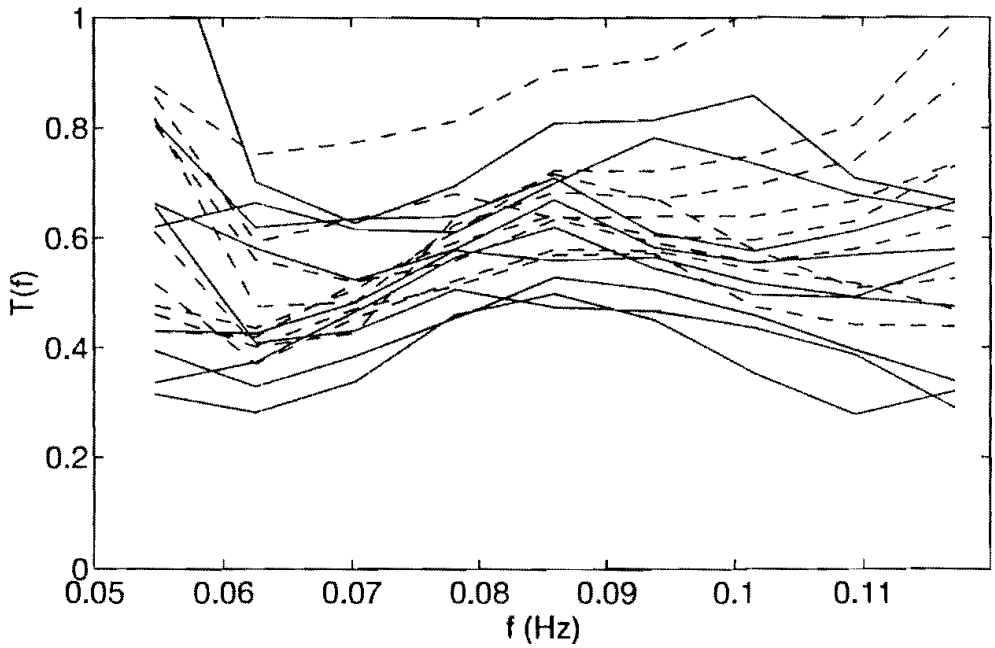

Figure 9.

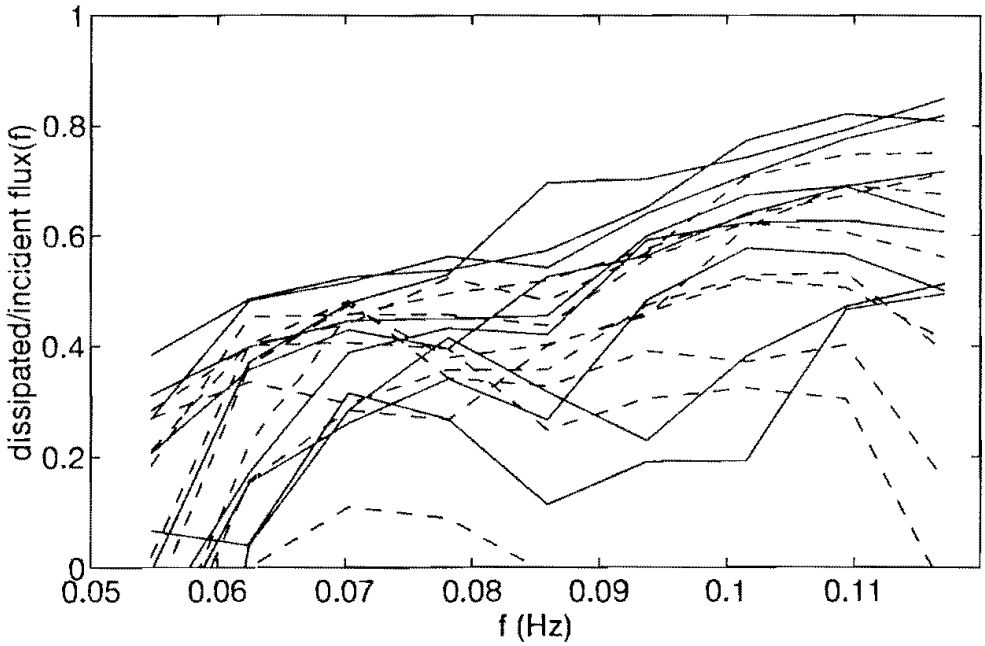
dissipated/incident flux(f)
f (Hz)
0
0.2
0.4
0.6
0.8
1
0.05
0.06
0.07
0.08
0.09
0.1
0.11

Figure 10.

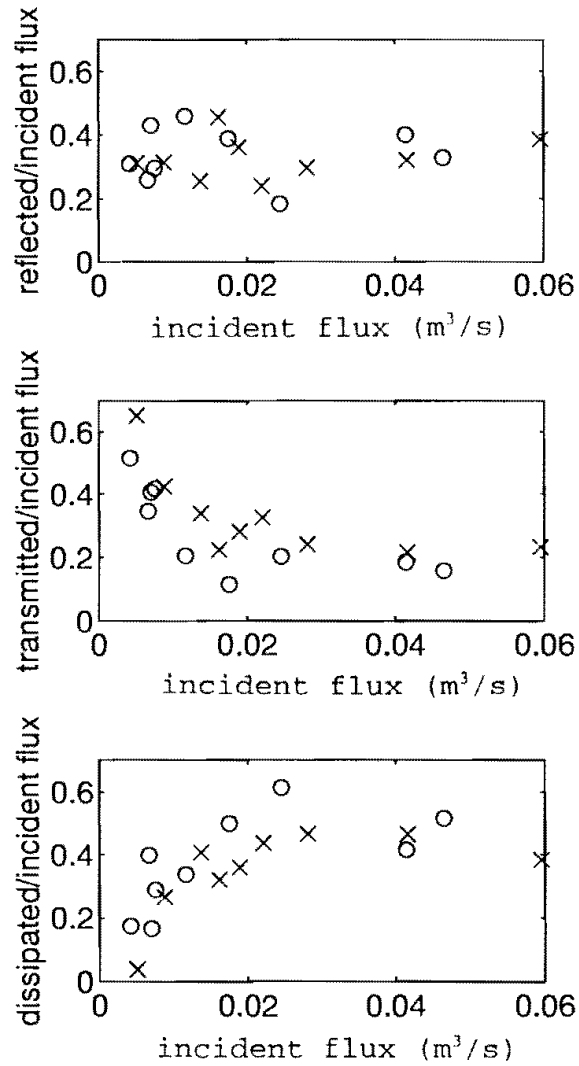
reflected/incident flux
0.6
0.4
0.2
0
0
0.02
0.04
0.06
incident flux (m³/s)
transmitted/incident flux
0.6
0.4
0.2
0
0
0.02
0.04
0.06
incident flux (m³/s)
dissipated/incident flux
0.6
0.4
0.2
0
0
0.02
0.04
0.06
incident flux (m³/s)

Figure 11.

REFERENCES

Goda, Y. and Y. Suzuki, 1976: "Estimation of Incident and Reflected Waves in Random Wave Experiments." *Proc. 15th. Int. Coastal Engineering Conf.*, ASCE, 828-845.

Isobe, M. and K. Kondo, 1984: "Method for Estimating Directional Wave Spectrum in Incident and Reflected Wave Field." *Proc. 19th Int. Coastal Engineering Conf.*, ASCE, 467-483.

Long, R. B. and K. Hasselmann, 1979: "A Variational Technique for Extracting Directional Spectra from Multi-component Wave Data." *J. Phys. Oceanogr.*, **9**(2), 373-381.

Mansard, E. P. D. and E. R. Funke, 1980: "The Measurement of Incident and Reflected Spectra Using a Least Squares Method." *Proc. 17th. Int. Coastal Engineering Conf.*, ASCE, 154-172.

Morden, D. B., E. P. Richey and D. R. Christensen, 1976: "Decomposition of Co-existing Random Wave Energy." *Proc. 15th. Int. Coastal Engineering Conf.*, ASCE, 846-865.

Okihiro, M., R. T. Guza and R. J. Seymour, 1992: "Bound Infragravity Waves." *J. Geophys. Res., 97,* 11,453-11,469.

Thornton, E. B. and R. J. Calhoun, 1972: "Spectral Resolution of Breakwater Reflected Waves." *Journal of the Waterways, Harbors and Coastal Engineering Division.*, ASCE, **98**, 443-460.

Yokoki, H., Isobe, M., and Watanabe, A. 1992. "A Method for Estimating Reflection Coefficient in Short-Crested Random Seas." *Proc. 23rd. Int Coastal Engineering Conf.*, ASCE, 765-776.

Zelt, J. A. and J. E. Skjelbreia, 1992: "Estimating Incident and Reflected Wave Fields Using an Arbitrary Number of Wave Gauges." *Proc. 23rd. Int. Coastal Engineering Conf.*, ASCE, 777-789.

INITIAL DISTRIBUTION LIST

1.	Defense Technical Information Center Cameron Station Alexandria, Virginia 22304-6145	2
2.	Library, Code 052 Naval Postgraduate School Monterey, California 93943-5002	2
3.	T. H. C. Herbers, Code OC/He Naval Postgraduate School Monterey, California 93943-5002	3
4.	E. B. Thornton, Code OC/Tm Naval Postgraduate School Monterey, California 93943-5002	2
5.	T. C. Lippmann, Code OC/Li Naval Postgraduate School Monterey, California 93943-5002	1
6.	W. S. Dickson Officer in Charge NAVTRAMETOC Det 400 Russell Ave NAS New Orleans, Louisiana 70143-5012	2
7.	T. Kendall San Francisco District U. S. Army Corps of Engineers 211 Main St. San Francisco, California 94105	1
8.	T. Bonigut San Francisco District U. S. Army Corps of Engineers 211 Main St. San Francisco, California 94105	2